CHEMISTRY
A EUROPEAN JOURNAL

DOI: 10.1002/chem.200902750

Self-Assembly of Discrete Homochiral, Helical, Hydrogen-Bonded Nanocages: From Vesicles to Microspheres and Tubules Capable of Gelating Solvents

Liwei Yan, Ying Xue, Ge Gao, Jingbo Lan, Fan Yang, Xiaoyu Su, and Jingsong You*[a]

Abstract: The chiral tris-monodentate imidazolinyl ligands **1a–c** exhibit a strong tendency to form the discrete, helical [2+3] nanocages **3** ([$\mathbf{1}_2$·$\mathbf{2}_3$]) with tartaric acids **2**. Circular dichroism (CD) spectra and theoretical calculations reveal that supramolecular handedness of capsulelike architectures is determined only by the chirality of the imidazolinyl ligands rather than tartaric acids. The chirality of imidazolinyl ligands is transferred to the helicity of the complexes through the directed hydrogen bonds between the N3 atom of imidazoline rings and the carboxyl of tartaric acids. These hydrogen-bonded nanocages can spontaneously self-assemble into spherical vesicles, during which the hydrogen bonding that arises from the hydroxyl groups of tartaric acids plays a crucial issue. The vesicles formed by [{(*S*,*S*,*S*)-**1a**}$_2$($\mathbf{2}^{L}$)$_3$] (**3a**) may further evolve into microspheres that gelate organic solvents after being aged at −20 °C for 24 h, and can also be unprecedentedly transformed to tubular assemblies capable of rigidifying the solvents when subjected to ultrasound irradiation.

Keywords: gels · nanocages · nanotubes · self-assembly · vesicles

Introduction

Three-dimensional cage/capsulelike supramolecular architectures formed by noncovalent interactions are currently gaining intensive attention due to their aesthetically appealing topologies and potential applications in host–guest chemistry and catalysis.[1] Although numerous reports continue to elucidate the details of preparation and characterization of nanometer-scale cages/capsules, considerably less is known about further aggregation and supramolecular assembly of these discrete entities in solutions. Recent studies have shown that larger spherical, vesicular, and tubular aggregates can be formed by self-assembled nanocapsules or nanocages. Atwood et al. described the supermolecular self-assembly of a near-spheroidal hexameric nanocapsule based on pyrogallol[4]arene into submicron spheres and tubules or combinations thereof.[2] Liu et al. demonstrated for the first time that the commercially available $[Pd_6L_4]^{12+}$ (Pd = ethylenediamine palladium(II), L = 2,4,6-tris(4-pyridyl)triazine) cationic metal–organic octahedral nanocages can self-assemble into monodisperse hollow vesicles in solution.[3]

Various biological or chemical assemblies including vesicles, tubules, fibrils, and viral helical coats perform numerous biochemical actions in nature. In particular, vesicles have achieved prominence due to their potential applications in biomimetic models, drug or gene carriers, and nanostructured materials, and so on.[4] Traditionally, vesicles consist of a variety of amphiphilic components.[5] In contrast, the design of vesicles with non-amphiphilic segments has been a challenging and fascinating field of research.[3,6]

Multimonodentate nitrogen-containing heterocyclic rings with arene cores have recently been of increasing interest in the design and construction of a variety of cagelike topologies.[1,7] Recently, we disclosed that the chiral tris-monodentate imidazolinyl ligand (*S*,*S*,*S*)-**1a** could preferentially form homochiral, helical sandwich-shaped architectures (*M*)-[M_3-{(*S*,*S*,*S*)-**1a**}$_2$] with a set of d^3–d^{10} transition-metal ions.[8] Herein we wish to report an unprecedented finding that the non-amphiphilic, homochiral, helical hydrogen-bonded [2+3] nanocages **3** ([$\mathbf{1}_2$·$\mathbf{2}_3$]), which are formed by self-assembly of the chiral C_3-tris(imidazoline) ligands **1** and tartaric acids **2** in a 2:3 ratio, may spontaneously aggregate into vesicles, and further evolve into microspheres and tubules capa-

[a] L. Yan, Prof. Dr. Y. Xue, Prof. Dr. G. Gao, Dr. J. Lan, F. Yang, Dr. X. Su, Prof. Dr. J. You
Key Laboratory of Green Chemistry and Technology of Ministry of Education
College of Chemistry, and State Key Laboratory of Biotherapy
West China Medical School, Sichuan University
29 Wangjiang Road, Chengdu 610064 (P.R. China)
Fax: (+86) 28-85412203
E-mail: jsyou@scu.edu.cn

Supporting information for this article is available on the WWW under http://dx.doi.org/10.1002/chem.200902750.

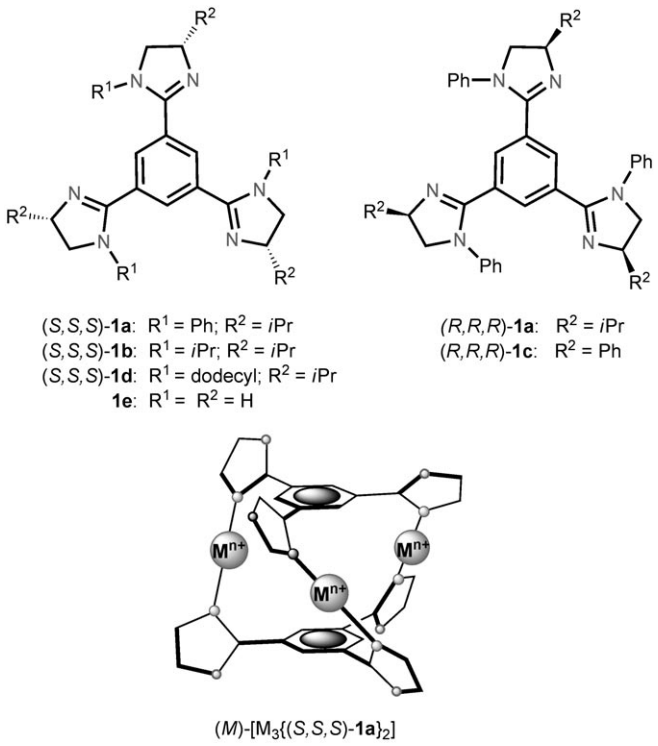

ble of gelating solvents when subjected to aging and an irradiation with ultrasound, respectively. This is a completely new phenomenon observed for hydrogen-bonded nanocages.

Results and Discussion

Synthesis and characterization of discrete hydrogen-bonded nanocages [1_2·2_3] (3): With the chiral C_3-tris(imidazoline) ligands in hand, the solution behavior of (*S,S,S*)-**1a** with L-tartaric acid ($\mathbf{2}^{L}$) was first investigated as the most studied example. We found that (*S,S,S*)-**1a** could exhibit a strong tendency to induce the generation of a discrete cage with $\mathbf{2}^{L}$ (Figure 1). The self-assembled nanocapsule [{(*S,S,S*)-**1a**}$_2$($\mathbf{2}^{L}$)$_3$] (**3a**) was prepared by the reaction of (*S,S,S*)-**1a** with $\mathbf{2}^{L}$ in a 2:3 ratio in methanol. Given that the ligand

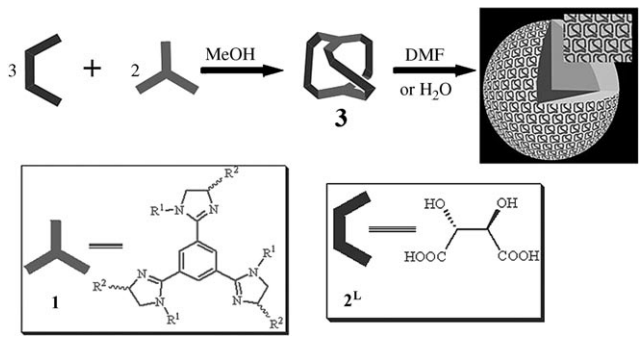

Figure 1. A schematic representation of the self-assembly of nanocapsules **3** ([$\mathbf{1}_2$·$\mathbf{2}_3$]).

(*S,S,S*)-**1a** is insoluble in [D_7]DMF and L-tartaric acid is insoluble in $CDCl_3$, the NMR spectroscopic studies were carried out in both of the deuterated solvents accordingly. The ^{1}H NMR spectra of **3a** in $CDCl_3$ showed one set of new signals in a simple, highly symmetrical pattern, and the signals for ligand (*S,S,S*)-**1a** disappeared completely, which clearly indicated the quantitative formation of a single self-assembled architecture (Figure 2a,b and Figure S22 in the Supporting Information). In [D_7]DMF, the chiral proton of $\mathbf{2}^{L}$ was strongly shifted upfield (Figure 2c–d). The self-assembled complex **3a** could be further confirmed by the electrospray ionization time-of-flight mass measurement (ESIMS TOF; Figure S5 in the Supporting Information). The ^{1}H and ^{13}C NMR spectroscopic studies in combination with ESIMS (TOF) measurements suggested that the other C_3-tris(imidazoline) ligands such as (*S,S,S*)-**1b** and (*R,R,R*)-**1c** could also form the [2+3] nanocages [{(*S,S,S*)-**1b**}$_2$($\mathbf{2}^{L}$)$_3$] and [{(*R,R,R*)-**1c**}$_2$($\mathbf{2}^{L}$)$_3$] (**3b** and **3c**, respectively) with L-tartaric acid (Figures S1, S2, S6, S7, S23, and S24 in the Supporting Information). However, when the R^1 group of the imidazoline ring was changed to the long chain, a diminished tendency to form cagelike architectures was observed with (*S,S,S*)-**1d** (Figure S27 in the Supporting Information). In addition, we also investigated the other diacids such as *m-*, *o-*, and *p*-phthalic acids, succinic acid, and oxalic acid, but found that they only created such [2+3] assemblies with difficulty.

We subsequently investigated the circular dichroism (CD) spectra of the self-assembled cages [$\mathbf{1a}_2$·$\mathbf{2}_3$] formed by (*S,S,S*)-**1a** or (*R,R,R*)-**1a** and three tartaric acids (**2**) including L-tartaric acid ($\mathbf{2}^{L}$), D-tartaric acid ($\mathbf{2}^{D}$), and *meso*-tartaric acid ($\mathbf{2}^{meso}$). More surprisingly, the signs of the CD signals were dependent only on the absolute configuration of ligands rather than tartaric acids, which was consistent with our previously reported helical metal complexes.[8] All the

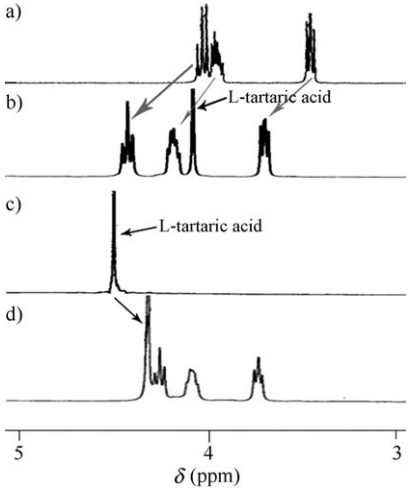

Figure 2. ^{1}H NMR spectra for L-tartaric acid with (*S,S,S*)-**1a** at 293 K: a) the ligand (*S,S,S*)-**1a** and b) (*S,S,S*)-**1a**/L-tartaric acid = 2:3 in $CDCl_3$ (6 mM). c) L-tartaric acid, and d) (*S,S,S*)-**1a**/L-tartaric acid = 2:3 in [D_7]DMF (6 mM).

assemblies formed by (*S*,*S*,*S*)-**1a** showed a negative Cotton effect similar to that of ligand (*S*,*S*,*S*)-**1a** (and vice versa; Figure 3).

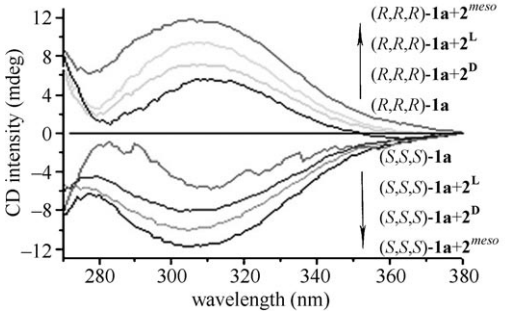

Figure 3. CD spectra of the assemblies [$\mathbf{1a}_2$·$\mathbf{2}_3$] derived from (*S*,*S*,*S*)-**1a** or (*R*,*R*,*R*)-**1a** and $\mathbf{2}^{L}$, $\mathbf{2}^{D}$, or $\mathbf{2}^{meso}$ in DMF (0.15 mM).

Molecular modeling: Theoretical calculations were performed to better understand the supramolecular organization in these structures. All calculations were carried out by using the Gaussian 03 program, and full geometry optimizations of the complexes [$\mathbf{1a}_2$·$\mathbf{2}_3$] were performed at the HF/STO-3G level of theory.[9] The stationary point was confirmed through the harmonic frequency analysis in the same basis set as a minimum with all positive frequencies. The optimized geometries of the complexes generated by (*S*,*S*,*S*)-**1a** with L-, D-, and *meso*-tartaric acids (denoted as [{(*S*,*S*,*S*)-$\mathbf{1a}$}$_2$($\mathbf{2}^{L}$)$_3$], [{(*S*,*S*,*S*)-$\mathbf{1a}$}$_2$($\mathbf{2}^{D}$)$_3$], and [{(*S*,*S*,*S*)-$\mathbf{1a}$}$_2$($\mathbf{2}^{meso}$)$_3$], respectively) are shown in Figure 4a–c (left). From Figure 4a–c (left), one can see that these complexes have similar left-handed structures, (*M*)-[{(*S*,*S*,*S*)-$\mathbf{1a}$}$_2$$\mathbf{2}_3$], which are held together with twelve directed hydrogen bonds to form the capsulelike assembly. The N···H distances in O–H···N hydrogen bonds between the −OH of the carboxyl groups of tartaric acids and the nitrogen atoms in the 3-position of the imidazoline rings are in the range from 1.671 to 1.721 Å. The O···H distances in C–H···O hydrogen bonds between the carbonyl groups (C=O) of tartaric acids and the aromatic hydrogen atoms of the central benzene rings are in the range from 2.040 to 2.260 Å. The two central benzene rings of (*S*,*S*,*S*)-**1a** lie nearly parallel to each other with interplane distances of 5.78, 5.82, and 5.69 Å for [{(*S*,*S*,*S*)-$\mathbf{1a}$}$_2$($\mathbf{2}^{L}$)$_3$], [{(*S*,*S*,*S*)-$\mathbf{1a}$}$_2$($\mathbf{2}^{D}$)$_3$], and [{(*S*,*S*,*S*)-$\mathbf{1a}$}$_2$($\mathbf{2}^{meso}$)$_3$], respectively. The imidazoline acceptors are directed toward the out-of-plane of the C_3-symmetric facial ligand, and the tilting angle of about 35° between the central benzene and the imidazoline ring gives rise to the curvature needed for the formation of a helical structure. It seems that the chirality of ligand **1a** is transferred to the helicity of the complex through the directed hydrogen bonds between **1a** and **2**. Therefore, it can be concluded that the *M* helicity is induced by (*S*,*S*,*S*)-**1a** rather than tartaric acids to afford (*M*)-[{(*S*,*S*,*S*)-$\mathbf{1a}$}$_2$$\mathbf{2}_3$], whereas the *P* helicity is induced by (*R*,*R*,*R*)-**1a** to afford (*P*)-[{(*R*,*R*,*R*)-$\mathbf{1a}$}$_2$$\mathbf{2}_3$] (Figure 4a–c (right)), which is in good

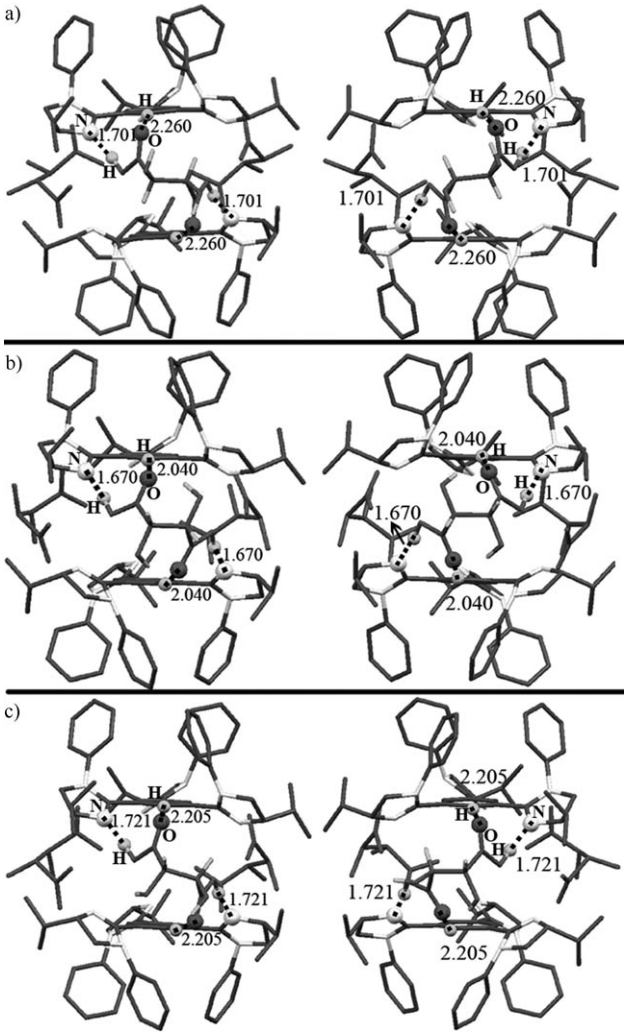

Figure 4. a) HF/STO-3G-calculated structures of enantiomers of (*M*)-[{(*S*,*S*,*S*)-$\mathbf{1a}$}$_2$($\mathbf{2}^{L}$)$_3$] (left) and (*P*)-[{(*R*,*R*,*R*)-$\mathbf{1a}$}$_2$($\mathbf{2}^{D}$)$_3$] (right). Hydrogen-bond lengths: O···H = 2.260, N···H = 1.701 Å. b) HF/STO-3G-calculated structures of enantiomers of (*M*)-[{(*S*,*S*,*S*)-$\mathbf{1a}$}$_2$($\mathbf{2}^{D}$)$_3$] (left) and (*P*)-[{(*R*,*R*,*R*)-$\mathbf{1a}$}$_2$($\mathbf{2}^{L}$)$_3$] (right). Hydrogen-bond lengths: O···H = 2.040, N···H = 1.671 Å. c) HF/STO-3G-calculated structures of enantiomers of (*M*)-[{(*S*,*S*,*S*)-$\mathbf{1a}$}$_2$($\mathbf{2}^{meso}$)$_3$] (left) and (*P*)-[{(*R*,*R*,*R*)-$\mathbf{1a}$}$_2$($\mathbf{2}^{meso}$)$_3$] (right). Hydrogen-bond lengths: O···H = 2.205, N···H = 1.721 Å. All hydrogen atoms except those at selected $^1/_3$ interacting sites are omitted for clarity. Hydrogen bonds viewed from the side are shown as dotted lines (for color figure, see Figure S28 in the Supporting Information).

accordance with the CD studies. It should be noted, however, that Hong et al. reported that the achiral tris-monodentate imidazolinyl ligand **1e** formed the helical [2+3] nanocages with D- or L-tartaric acid in aqueous solvents, and the handedness of the cages was induced by the chiral tartaric acids through charged hydrogen bonds.[10]

For the *M*-type helical supramolecular self-assembled capsules (*M*)-[{(*S*,*S*,*S*)-$\mathbf{1a}$}$_2$$\mathbf{2}_3$], the approximation HF/STO-3G method yielded the relative electronic energies of [{(*S*,*S*,*S*)-$\mathbf{1a}$}$_2$($\mathbf{2}^{D}$)$_3$] (0.0 kcal mol^{-1}), [{(*S*,*S*,*S*)-$\mathbf{1a}$}$_2$($\mathbf{2}^{meso}$)$_3$] (7.3 kcal mol^{-1}), and [{(*S*,*S*,*S*)-$\mathbf{1a}$}$_2$($\mathbf{2}^{L}$)$_3$] (15.4 kcal mol^{-1}). For the *P*-type helical structures, the relative electronic energies of

$[\{(R,R,R)\text{-}\mathbf{1a}\}_2(\mathbf{2}^{L})_3]$, $[\{(R,R,R)\text{-}\mathbf{1a}\}_2(\mathbf{2}^{meso})_3]$, and $[\{(R,R,R)\text{-}\mathbf{1a}\}_2(\mathbf{2}^{D})_3]$ are 0.0, 7.3, and 15.4 kcal mol^{-1}, respectively. It can be also seen from Figure 4a–c and their relative electronic energies that the complexes $[\{(R,R,R)\text{-}\mathbf{1a}\}_2(\mathbf{2}^{D})_3]$, $[\{(R,R,R)\text{-}\mathbf{1a}\}_2(\mathbf{2}^{L})_3]$, and $[\{(R,R,R)\text{-}\mathbf{1a}\}_2(\mathbf{2}^{meso})_3]$ are the corresponding enantiomers of $[\{(S,S,S)\text{-}\mathbf{1a}\}_2(\mathbf{2}^{L})_3]$, $[\{(S,S,S)\text{-}\mathbf{1a}\}_2(\mathbf{2}^{D})_3]$, and $[\{(S,S,S)\text{-}\mathbf{1a}\}_2(\mathbf{2}^{meso})_3]$, respectively.

Vesicular aggregates: We further aimed at exploration of the aggregation behavior of these discrete hydrogen-bonded capsules **3a–c** and **3e** ($[\mathbf{1e}_2{\cdot}(\mathbf{2}^{L})_3]$) in solution. Atomic force microscopy (AFM) was first conducted to investigate the self-assembly behavior. The AFM images clearly revealed that **3a–c** and **3e** spontaneously self-assembled into spherical particles with uniform shape and size in DMF (Figure 5a–d). The average diameters of the particles of **3a–c** and **3e** estimated from the fitted histograms of the size distribution after subtracting the tip-broadening parameters were 29.3, 370, 122, and 190 nm, respectively (Figure S15 in the Supporting Information).[11] Taking **3a** as an example, the histogram obtained from the individual diameters of 300 particles shows a Lorentzian distribution ($R^2 = 0.9658$) with an average size of 29.3 nm and full width at half-maximum (fwhm) of 8.8 nm (Figure 5e). The ratios of the diameter and height of aggregates formed by **3a–c** and **3e** were estimated to be aorund 7, 57, 11, and 39, respectively, which indicated a considerable flattening of the spheres, presumably as a result of either the removal of the solvent after the transfer of the nanosized assemblies from solution to a mica surface or the high local force exerted by the AFM tip (Figures S11–S14 in the Supporting Information).[5c,6,12] Further dynamic light scattering (DLS) experiments with **3a** confirmed the formation of supermolecular aggregates with an average diameter of 28.5 nm (Figure 5f), which was in agreement with the AFM study. Moreover, the spherical assemblies displayed a narrow size distribution, which was indicative of the formation of well-equilibrated structures. Controlled experiments with either $\mathbf{2}^{L}$ or ligands **1** in DMF ruled out any artifacts, which revealed that the presence of both components was essential for the formation of spherical particles.

More interestingly, the hollow vesicular feature of the self-assembled spheres of **3a** in DMF was observed in the transmission electron microscopy (TEM) images (Figure 6a). The average diameter of spherical vesicles was in accordance with the AFM and DLS studies. The TEM images without staining revealed the contrast difference between the periphery and the inner part of the spheres, which is expected from the 2D projection of 3D vesicular structures

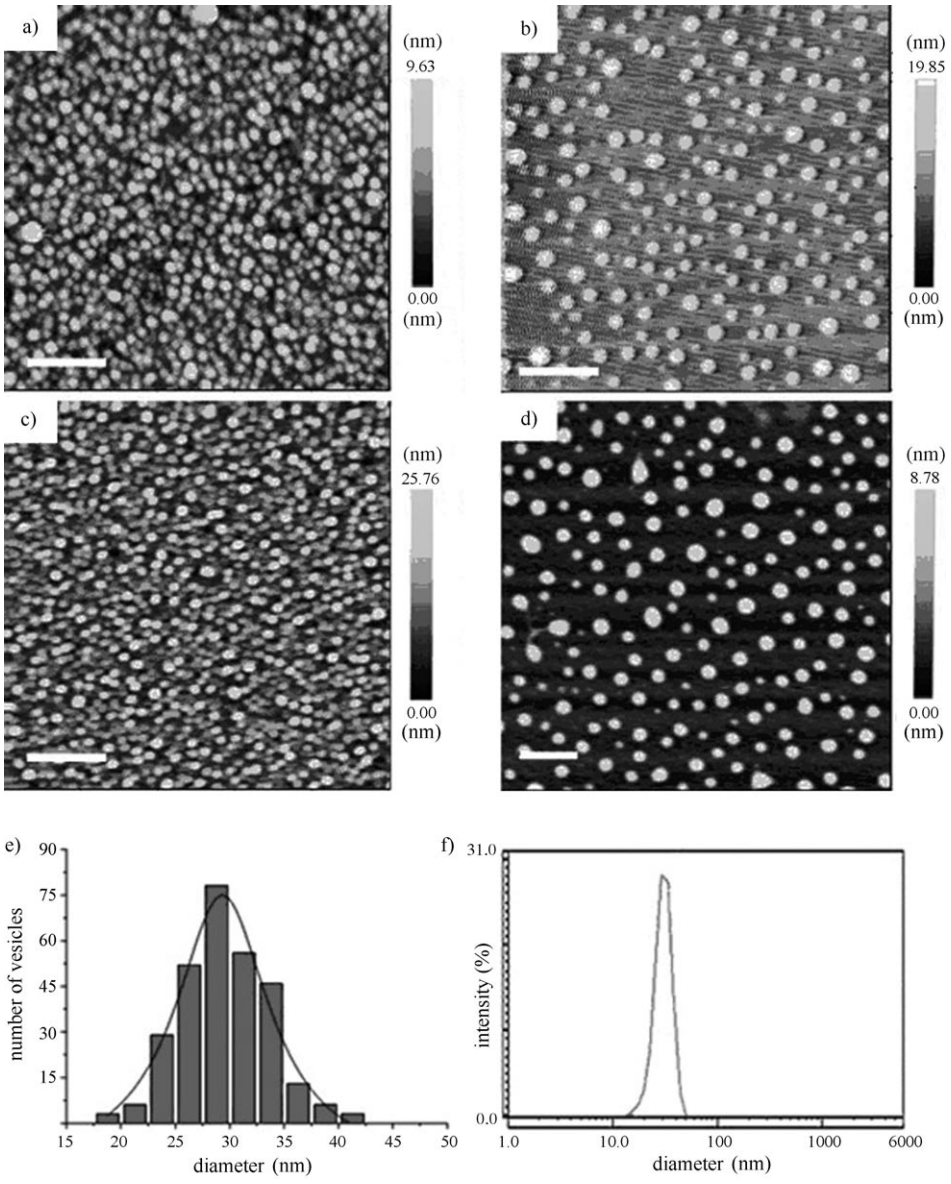

Figure 5. Tapping-mode AFM height images of aggregates formed from a) **3a** in DMF (5 mM), b) **3b** in DMF (5 mM), c) **3c** in DMF (5 mM), and d) **3e** in H_2O (5 mM) on a freshly cleaved mica surface after the solvent was evaporated (scale bar: a) 200 nm, b) 2 μm, c) 1 μm, d) 1 μm), and e) the corresponding histogram (Lorentzian fit) of **3a**. f) The intensity-weighted distribution of the aggregates obtained from the DLS measurement of the sample of **3a** (5 mM) in DMF at 25 °C.

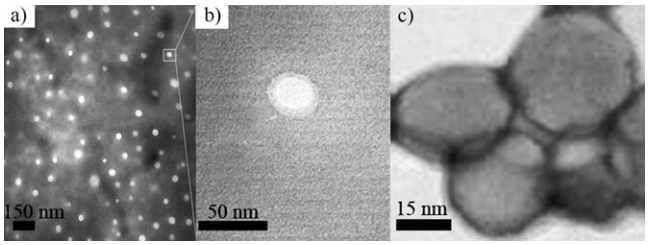

Figure 6. a) TEM images (unstained) of **3a** in DMF (5 mM) on a carbon-coated copper grid, and b) an enlarged image of the area marked in (a). c) TEM image of **3a** in DMF (5 mM) on a carbon-coated copper grid stained with phosphotungstic acid aqueous solution (10 g dm^{-3}).

typically observed by TEM. The structure is clear from a magnified image of a vesicle (Figure 6b). Notably, the images taken from samples cast from solutions in DMF remained intact even after 45 days.

To further shed light on whether the vesicular aggregates were composed of the discrete hydrogen-bonded capsule **3a**,[2,10] metal-coordinated nanocage [{(*S*,*S*,*S*)-**1a**}$_2$Cu$_3$Cl$_6$] was investigated using TEM because its structure has proven incapable of disassembly in the solvent systems employed.[8] As depicted in Figure 7, the spherical aggregates with an average diameter of 20 nm were observed, although the images were obviously darker, presumably due to the high content of heavy metal ions in the resultant superstructures. Therefore, in combination with the ESIMS (TOF) results, it is reasonable to assume that the vesicular objects illustrated in Figure 6 consist of a number of discrete capsules **3a**.

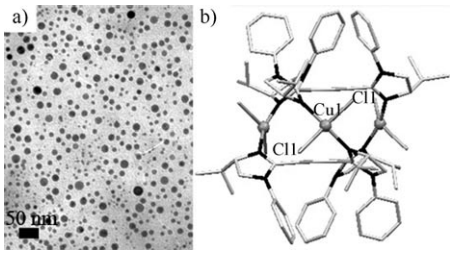

Figure 7. a) TEM image (unstained) of nanocages [{(*S*,*S*,*S*)-**1a**}$_2$Cu$_3$Cl$_6$] (5 mM) in DMF. b) The crystal structure of [{(*S*,*S*,*S*)-**1a**}$_2$Cu$_3$Cl$_6$]. Atom color code: C (light gray), N (black), Cu (dark gray), and Cl (gray); H is omitted.

We further investigated in detail the influence of the ratio of the two components on the aggregation by ^{1}H NMR spectroscopic and microscopy studies. We found that both cages and vesicles started to become less prevalent as the ratio of the tris-monodentate imidazolinyl ligand and tartaric acid changed away from 2:3, which also clearly indicated that the cage structure is important to the formation of vesicles. Although the specific interactions between these capsules are not clear at this stage, we rationalized that the spherical vesicles might be stabilized by numerous subtle noncovalent interactions such as neighboring cooperative intermolecular hydrogen bonding, van der Waals, and π–π stacking interactions.

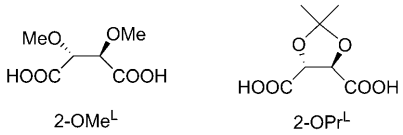

To get insight into the noncovalent interactions that actually influence the aggregation, the two hydroxyl groups of **2**^{L} were blocked to form the ether derivative 2-OMe^L and the ketal derivative 2-OPr^L. Similar to **2**^{L}, the NMR spectroscopic and ESIMS (TOF) studies revealed that both of the two L-tartaric acid derivatives could quantitatively generate the [2+3] nanocages with (*S*,*S*,*S*)-**1a** (Figures S3, S4, S8, S9, S25, and S26 in the Supporting Information). However, these capsulelike supramolecular architectures were not capable of evolving into any clear and uniform vesicular assemblies (Figure S16 in the Supporting Information). These observations distinctly demonstrated that hydrogen bonding from the hydroxyl groups of tartaric acids played a key role in the formation of vesicular aggregates.

Gelation of nanocages: Subsequently, the size of the aggregates of capsules was observed to be dependent upon the concentration of the solution. Higher concentrations could result in larger spherical aggregates. Taking **3a** as the representative example, TEM images indicated an increase in the size of the vesicular aggregates from approximately 30 to 200 nm as the concentration of **3a** in DMF increased from 5 to 29 mM (Figures 6 and 8a). As illustrated in Figure 8a, the

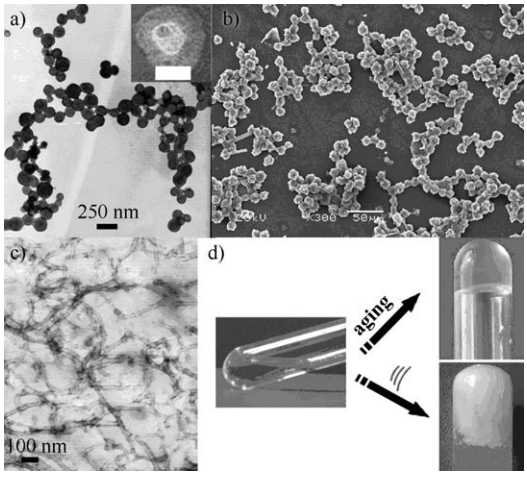

Figure 8. a) TEM image of **3a** (29 mM) in DMF on a carbon-coated copper grid, stained with phosphotungstic acid aqueous solution (10 g dm^{-3}). Inset: TEM image of unstained **3a** (scale bar: 100 nm). b) SEM image of the sample of **3a** in DMF (29 mM, aged at −20 °C for 24 h) on a mica surface after the solvent was evaporated. c) TEM image (unstained) of **3a** (29 mM) in DMF after sonication. d) Photographs of a solution of **3a** at room temperature (left), a transparent gel of **3a** after being aged at −20 °C for 24 h (right top), and an opaque gel of **3a** after sonication (right bottom) in DMF (29 mM).

large vesicular aggregates interconnected to form "pearls on a string." More interestingly, after the samples of **3a** were subjected to aging in DMF or *N*,*N*-dimethylacetamide (DMA) at −20 °C for 24 h, transparent gels were seen with a critical gelation concentration (CGC) of 2 wt % (Figure 8d). The scanning electron microscopy (SEM) image of **3a** (29 mM) revealed that aging of the solution resulted in the formation of uniform spherical aggregates with a size of around 10 μm, many of which were observed to be adhered together (Figure 8b). We speculated that the large particles should be attributed to the spontaneous fusion of the smaller ones after aging.[6a,13] Subsequently, these strings of microspheres created a continuous interconnected globular network that rigidified the solvent DMF (Figure 9). This class

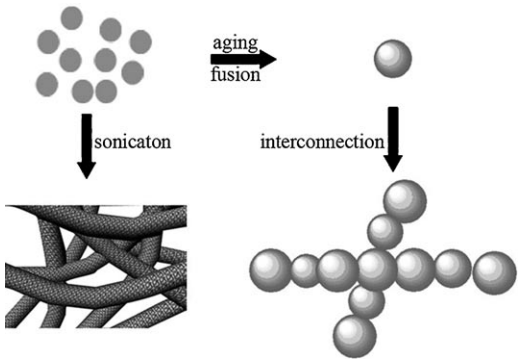

Figure 9. A schematic representation of the self-assembly of vesicles **3a**.

of gelation is unusual, as most previously reported examples are based on self-aggregation of gelator molecules into long, entangled fibrous networks.[14] As far as we know, there are no reports on discrete hydrogen-bonded nanocages that can develop into organogels through microspheres. In addition, further investigation demonstrated that the capsulelike assemblies formed by 2-OMe^{L} or 2-OPr^{L} that lacked free hydroxyl groups were not only incapable of generating vesicular aggregates described above, but also could not evolve into gelators.

Alternatively, as the self-assembled spheres of **3a** were submitted to sonication (0.45 W cm^{-2}, 40 KHz) in DMF for a period of 1–3 min, a complete and homogeneous liquid gelation was also observed. This opaque white gel formed could be stable for several months at room temperature without visible changes (Figure 8d). The resulting gel was thermoreversible, as the gel feature could be lost upon heating to more than 45 °C. In the case of DMF, 1 g of **3a** was capable of immobilizing 50 g of solvent (CGC = 2 wt %). Similarly, the gelation of **3a** was also observed in *N*,*N*-dimethyl acetamide (DMA). However, **3b–e** containing only alkyl-, aryl-, or lacking substituted groups on the imidazoline rings did not undergo gelation, thereby indicating that both of the van der Waals and π–π stacking interactions that arise from the alkyl and aryl segments are indispensable to establish the gel.[15]

To our surprise, transmission electron microscopy (TEM) clearly revealed a dramatic morphological transformation of the sample **3a** after sonication. As shown in Figure 8c, the TEM image obtained from the gel in DMF indicated the presence of well-grown distinct cylindrical assemblies with diameters of approximately 25 nm, which are responsible for gelation (Figure 9). The clear contrast between the interior and periphery of the unstained cylindrical structures is characteristic of the projection images of hollow tubular aggregates. In spite of a few reports on morphological transformation between the vesicular and tubular structures,[11b,16] it is notable that there are no examples that describe such an ultrasound-induced switching of morphologies of supramolecular aggregates of hydrogen-bonded nanocages. To further investigate the fundamental building blocks of the macroscopic gel-phase network, ESIMS (TOF) spectra of gels expedited by aging or sonication were recorded accordingly. Despite the different morphologies, their mass spectra showed a main peak at *m*/*z* 1722.7 that was assigned to the species [{(*S*,*S*,*S*)-**1a**}$_2$(**2**^{L})$_3$], clearly revealing that the cagelike supramolecular structures were still present (Figure S10 in the Supporting Information).

Conventionally, supramolecular gels are prepared by heating a gelator in an appropriate solvent and subsequently cooling the resulting isotropic supersaturated solution to room temperature.[17] Since Naota et al. observed ultrasound-triggered gelation for the first time,[18] the employment of sonication as an unexpected but effective stimulus to metal coordination, hydrogen bonding, π–π stacking, and/or van der Waals interaction-dependent molecular gels has received unprecedented attention.[19] We recently also demonstrated a new gelation mechanism based on a coordination polymer, in which ultrasound changes the morphology of the material from sheetlike microparticles into nanofibers.[20] To our knowledge, that was the first example that described the ultrasound-induced gelation through the formation of tubular architectures composed of the discrete supramolecular nanocages, although several multicomponent gelators containing tartaric acids that show fibrillar, tubular, and ribbonlike morphologies have been reported.[21]

Conclusion

In conclusion, we have described that chiral tris-monodentate imidazolinyl ligands together with tartaric acids self-assembled into discrete, helical, hydrogen-bonded [2+3] nanocages, the handedness of which was determined only by the chirality of the imidazolinyl ligands. These non-amphiphilic cagelike supramolecular architectures then spontaneously aggregated into vesicles, and further evolved into microspheres that could gelate organic solvents after aging at −20 °C. These vesicles could also be transformed to tubular assemblies that resulted in the immobilization of solvents when subjected to irradiation with ultrasound. Efforts are now in progress to investigate the full scope of the transformation and to apply this strategy to other noncovalent sys-

tems. The work may open the door for the design of a new generation of vesicles from non-amphiphilic architectures.

Experimental Section

General remarks: ^{1}H NMR spectra were obtained using a Bruker AV-400 (400 MHz), a Varian Inova-400 (400 MHz), or a Varian INOVA-600 (600 MHz) instrument, whereas ^{13}C NMR spectra were recorded using a Bruker AV-400 (100 MHz), a Varian Inova-400 (100 MHz), or a Bruker AV-600 (150 MHz) instrument. The ^{1}H and ^{13}C NMR spectroscopic chemical shifts were measured relative to $CDCl_3$, $(CD_3)_2CO$, CD_3OD, or $[D_7]$DMF as the internal references. High-resolution (HR) MS were recorded using a Waters-TOF Premier mass spectrometer by positive ESI-Q-TOF. The optical rotations were determined using a WZZ-2B polarimeter or Rudolph Autopol V polarimeter. Elemental analyses were performed using a CARLO ERBA1106 instrument or a Heraeus CHN-O-RAPID instrument. Melting points were determined and are uncorrected. DLS experiments were recorded using a HORIBA LB-550 instrument. SEM images were obtained using a JSM-5900LV instrument at 20 kV. TEM studies were carried out using a JEM-100CXII (Figure S16 in the Supporting Information) or a HITACHI H-600 (others) instrument, operating at 100 kV. Tapping mode AFM imaging was performed under ambient conditions using a SEIKO SPA400 instrument by using BS-Tap 300Al levers (Budget Sensors, silicone cantilevers). Ultrasound irradiation was performed using a KQ3200 ultrasound bath (40 kHz, 0.45 W cm^{-2}). Unless otherwise noted, all reagents were obtained from commercial suppliers and used without further purification. Unless otherwise indicated, all syntheses and manipulations were carried out under a dry N_2 atmosphere. Anhydrous solvents were dried by standard procedures. 1,3,5-Tris(4,5-dihydro-1*H*-imidazol-2-yl)benzene (**1e**) and the complex **3e** were prepared by literature procedures.[10a,22] The chiral C_3-tris(imidazoline) ligands (*S*,*S*,*S*)-**1a** and (*R*,*R*,*R*)-**1a** were synthesized according to our previously reported methods.[8] (2*R*,3*R*)-2,3-Dimethoxysuccinic acid (2-OMe^L) and (4*R*,5*R*)-2,2-dimethyl-1,3-dioxolane-4,5-dicarboxylic acid (2-OPr^L) were synthesized by following literature procedures.[23]

Preparation of samples for AFM: Samples of **3a**–**c** (5 mM) in DMF and **3e** (5 mM) in H_2O were cast onto a freshly cleaved mica surface under ambient conditions, and then dried at 55 °C for 0.5 h before making AFM images.

Preparation of samples for TEM: TEM specimens were prepared by gently placing a carbon-coated copper grid on a surface of the sample. The TEM grid was removed, dried for 0.5 h at room temperature, and then subjected to observation.

Preparation of samples for SEM: Samples of **3a** in DMF were placed on a freshly cleaved mica surface, left open to the atmosphere for drying, shielded with gold, and then examined.

Gelation tests: A capped vial was charged with complex **3a** (10.0 mg) dispersed in DMF (0.5 mL). The resulting mixture was aged at −20 °C for 24 h. The sample was simply confirmed by the "stable-to-inversion of a test tube" method. Similarly, the gelation of **3a** was observed in *N*,*N*-dimethylacetamide (DMA).

A capped vial was charged with complex **3a** (10.0 mg) dispersed in DMF (0.5 mL), and the mixture was then introduced into an ultrasonic cleaner (0.45 W cm^{-2}, 40 kHz) and submitted to sonication at 298 K for around 1–3 min. The sample was simply confirmed by the "stable-to-inversion of a test tube" method. Similarly, the gelation of **3a** was observed in DMA.

General procedures for the preparation of the chiral tris(imidazoline) ligands 1b–d:[8] (For synthetic routes, see Scheme S1 in the Supporting Information.) A solution of benzene-1,3,5-tricarbonyl trichloride **4** (4.8 g, 18 mmol) in CH_2Cl_2 (80 mL) was added dropwise to a stirred solution of amino alcohol (56 mmol) and triethylamine (9.4 mL, 68 mmol) in CH_2Cl_2 (80 mL) at 0 °C. The reaction mixture was then allowed to warm to room temperature, and stirring was continued for 12 h, followed by addition of water (100 mL). The mixture was filtered to give the corresponding tris-amido alcohol **5** as a white solid. A solution of **5** (10.8 mmol) in $SOCl_2$ (20 mL) was stirred at reflux for 10 h, and volatiles were then removed under reduced pressure to afford compound **6**. CH_2Cl_2 (60 mL), Et_3N (14.0 mL, 100 mmol), and amine (35.5 mmol) were added to the residue at 0 °C. The resulting mixture was allowed to warm to room temperature and stirred for 24 h. The solution was then washed with NaOH (10%, 50 mL) and the aqueous layer was extracted with CH_2Cl_2 (3×60 mL). The combined organic layers were dried over $MgSO_4$, and the solvent was removed in vacuo to give a yellow solid, which could be purified by column chromatography on silica gel.

Compound (*S*,*S*,*S*)-1b: Starting materials were (*S*)-valinol and isopropylamine. Compound (*S*,*S*,*S*)-**1b** was obtained in an 88% yield as a pale yellow semisolid after purification by column chromatography on silica gel with elution with ethyl acetate/methanol (6:1). $[\alpha]_D^{25}=67.8$ ($c=0.5$ in MeOH); ^{1}H NMR (400 MHz, $CDCl_3$): $\delta=0.92$ (d, $J=6.8$ Hz, 9H), 0.99 (d, $J=6.4$ Hz, 18H), 1.10 (d, $J=6.8$ Hz, 9H), 1.84–1.87 (m, 3H), 3.14 (t, $J=9.2$ Hz, 3H), 3.44 (t, $J=5.2$ Hz, 3H), 3.74–3.77 (m, 3H), 3.87–3.94 (m, 3H), 7.65 ppm (s, 3H); ^{13}C NMR (100 MHz, $CDCl_3$): $\delta=17.8$, 18.6, 19.3, 20.6, 33.2, 45.1, 46.6, 69.3, 128.9, 132.2, 164.0 ppm; ESIMS (TOF): *m*/*z*: 534.4 $[M]^+$; elemental analysis calcd (%) for $C_{33}H_{54}N_6$: C 74.11, H 10.18, N 15.71; found: C 74.07, H 10.28, N 15.58.

Compound (*R*,*R*,*R*)-1c: Starting materials were (*R*)-2-amino-2-phenylethanol and aniline. Compound (*R*,*R*,*R*)-**1c** was obtained in a 90% yield as a white solid after purification by column chromatography on silica gel with elution with ethyl acetate/methanol (5:1). M.p. 282–284 °C; $[\alpha]_D^{25}=-159.0$ ($c=0.5$ in MeOH); ^{1}H NMR (400 MHz, $CDCl_3$): $\delta=3.79$ (t, $J=8.4$ Hz, 3H), 4.37 (t, $J=10.0$ Hz,3H), 5.25 (2d, $J=8.0$ Hz, 8.0 Hz, 3H), 6.70 (d, $J=8.0$ Hz, 6H), 7.06–7.14 (m, 24H), 7.82 ppm (s, 3H); ^{13}C NMR (100 MHz, $CDCl_3$): $\delta=61.8$, 67.8, 123.3, 124.0, 126.7, 127.3, 128.7, 128.8, 130.8, 131.6, 142.7, 143.7, 161.3 ppm; ESIMS (TOF): *m*/*z*: 739.4 $[M+H]^+$; elemental analysis calcd (%) for $C_{51}H_{42}N_6$: C 82.90, H 5.73, N 11.37; found: C 82.84, H 5.88, N 11.27.

Compound (*S*,*S*,*S*)-1d: Starting materials were (*S*)-valinol and dodecylamine. Compound (*S*,*S*,*S*)-**1d** was obtained in a 50% yield as a pale yellow oil after purification by column chromatography on silica gel with elution with ethyl acetate/methanol (10:1). $[\alpha]_D^{25}=47.6$ ($c=0.5$ in MeOH); ^{1}H NMR (400 MHz, $CDCl_3$): $\delta=0.88$ (t, $J=7.2$ Hz, 9H), 0.93 (d, $J=6.8$ Hz, 9H), 1.02 (d, $J=6.8$ Hz, 9H), 1.26–1.34 (m, 54H), 1.47–1.50 (m, 6H), 1.84–1.89 (m, 3H), 2.80–2.83 (m, 3H), 2.98 (t, $J=9.2$ Hz, 3H), 3.06–3.13 (m, 3H), 3.56 (t, $J=10.0$ Hz, 3H), 3.88–3.95 (m, 3H), 7.72 ppm (s, 3H); ^{13}C NMR (100 MHz, $CDCl_3$): $\delta=14.1$, 18.1, 19.0, 22.7, 26.8, 29.1, 29.4, 29.5, 29.59, 29.61, 29.63, 29.67, 31.9, 33.3, 49.4, 53.4, 70.5, 129.3, 132.4, 165.4 ppm; ESI-HRMS (TOF): *m*/*z*: calcd for $C_{60}H_{109}N_6$ $[M+H]^+$: 913.8714; found: 913.8710.

Acknowledgements

This work was supported by grants from the National Natural Science Foundation of China (nos. 20702035 and 20602027). We thank the Centre of Testing and Analysis, Sichuan University for AFM, TEM, SEM, and NMR spectroscopic measurements.

[1] a) S. R. Seidel, P. J. Stang, *Acc. Chem. Res.* **2002**, *35*, 972; b) M. Fujita, M. Tominaga, A. Hori, B. Therrien, *Acc. Chem. Res.* **2005**, *38*, 369; c) D. Fiedler, D. H. Leung, R. G. Bergman, K. N. Raymond, *Acc. Chem. Res.* **2005**, *38*, 351; d) J. Rebek, Jr., *Angew. Chem.* **2005**, *117*, 2104; *Angew. Chem. Int. Ed.* **2005**, *44*, 2068; e) A. Lützen, *Angew. Chem.* **2005**, *117*, 1022; *Angew. Chem. Int. Ed.* **2005**, *44*, 1000; f) B. H. Northrop, Y.-R. Zheng, K.-W. Chi, P. J. Stang, *Acc. Chem. Res.* **2009**, *42*, 1554.

[2] M. W. Heaven, G. W. V. Cave, R. M. McKinlay, J. Antesberger, S. J. Dalgarno, P. K. Thallapally, J. L. Atwood, *Angew. Chem.* **2006**, *118*, 6367; *Angew. Chem. Int. Ed.* **2006**, *45*, 6221.

[3] D. Li, J. Zhang, K. Landskron, T. Liu, *J. Am. Chem. Soc.* **2008**, *130*, 4226.

[4] a) R. Blumenthal, M. J. Clague, S. R. Durell, R. M. Epand, *Chem. Rev.* **2003**, *103*, 53; b) D. E. Discher, A. Eisenberg, *Science* **2002**, *297*, 967; c) A. Mueller, D. F. O'Brien, *Chem. Rev.* **2002**, *102*, 727; d) U. Scherf, A. Gutacker, N. Koenen, *Acc. Chem. Res.* **2008**, *41*, 1086.

[5] For selected recent examples, see: a) Y. Li, X. Li, Y. Li, H. Liu, S. Wang, H. Gan, J. Li, N. Wang, X. He, D. Zhu, *Angew. Chem.* **2006**, *118*, 3721; *Angew. Chem. Int. Ed.* **2006**, *45*, 3639; b) S. H. Seo, J. Y. Chang, G. N. Tew, *Angew. Chem.* **2006**, *118*, 7688; *Angew. Chem. Int. Ed.* **2006**, *45*, 7526; c) C. Schmuck, T. Rehm, K. Klein, F. Gröhn, *Angew. Chem.* **2007**, *119*, 1723; *Angew. Chem. Int. Ed.* **2007**, *46*, 1693; d) X. Zhang, Z. Chen, F. Würthner, *J. Am. Chem. Soc.* **2007**, *129*, 4886; e) H. C. Shum, J.-W. Kim, D. A. Weitz, *J. Am. Chem. Soc.* **2008**, *130*, 9543; f) J. Zhang, Y.-F. Song, L. Cronin, T. Liu, *J. Am. Chem. Soc.* **2008**, *130*, 14408.

[6] a) A. Ajayaghosh, R. Varghese, V. K. Praveen, S. Mahesh, *Angew. Chem.* **2006**, *118*, 3339; *Angew. Chem. Int. Ed.* **2006**, *45*, 3261; b) A. Ajayaghosh, P. Chithra, R. Varghese, *Angew. Chem.* **2007**, *119*, 234; *Angew. Chem. Int. Ed.* **2007**, *46*, 230; c) W. Cai, G.-T. Wang, Y.-X. Xu, X.-K. Jiang, Z.-T. Li, *J. Am. Chem. Soc.* **2008**, *130*, 6936.

[7] For selected quite recent examples, see: a) S. Hiraoka, T. Tanaka, M. Shionoya, *J. Am. Chem. Soc.* **2006**, *128*, 13038; b) Y. Nishioka, T. Yamaguchi, M. Kawano, M. Fujita, *J. Am. Chem. Soc.* **2008**, *130*, 8160; c) T. Yamaguchi, M. Fujita, *Angew. Chem.* **2008**, *120*, 2097; *Angew. Chem. Int. Ed.* **2008**, *47*, 2067; d) K. Ghosh, J. Hu, H. S. White, P. J. Stang, *J. Am. Chem. Soc.* **2009**, *131*, 6695; e) S. Hiraoka, Y. Yamauchi, R. Arakane, M. Shionoya, *J. Am. Chem. Soc.* **2009**, *131*, 11646; f) K. Ono, J. K. Klosterman, M. Yoshizawa, K. Sekiguchi, T. Tahara, M. Fujita, *J. Am. Chem. Soc.* **2009**, *131*, 12526; g) S. Hiraoka, M. Goda, M. Shionoya, *J. Am. Chem. Soc.* **2009**, *131*, 4592; h) J. Lee, K. Ghosh, P. J. Stang, *J. Am. Chem. Soc.* **2009**, *131*, 12028.

[8] L. Yan, Z. Wang, M.-T. Chen, N. Wu, J. Lan, X. Gao, J. You, H.-M. Gau, C.-T. Chen, *Chem. Eur. J.* **2008**, *14*, 11601. CCDC-690674 ([{(*S*,*S*,*S*)-**1a**}$_2$Cu$_3$Cl$_6$]) contains the supplementary crystallographic data for this paper. These data can be obtained free of charge from The Cambridge Crystallographic Data Centre via www.ccdc.cam.ac.uk/data_request/cif.

[9] Gaussian 03, Revision D.01, M. J. Frisch, G. W. Trucks, H. B. Schlegel, G. E. Scuseria, M. A. Robb, J. R. Cheeseman, J. A. Montgomery, Jr., T. Vreven, K. N. Kudin, J. C. Burant, J. M. Millam, S. S. Iyengar, J. Tomasi, V. Barone, B. Mennucci, M. Cossi, G. Scalmani, N. Rega, G. A. Petersson, H. Nakatsuji, M. Hada, M. Ehara, K. Toyota, R. Fukuda, J. Hasegawa, M. Ishida, T. Nakajima, Y. Honda, O. Kitao, H. Nakai, M. Klene, X. Li, J. E. Knox, H. P. Hratchian, J. B. Cross, V. Bakken, C. Adamo, J. Jaramillo, R. Gomperts, R. E. Stratmann, O. Yazyev, A. J. Austin, R. Cammi, C. Pomelli, J. W. Ochterski, P. Y. Ayala, K. Morokuma, G. A. Voth, P. Salvador, J. J. Dannenberg, V. G. Zakrzewski, S. Dapprich, A. D. Daniels, M. C. Strain, O. Farkas, D. K. Malick, A. D. Rabuck, K. Raghavachari, J. B. Foresman, J. V. Ortiz, Q. Cui, A. G. Baboul, S. Clifford, J. Cioslowski, B. B. Stefanov, G. Liu, A. Liashenko, P. Piskorz, I. Komaromi, R. L. Martin, D. J. Fox, T. Keith, M. A. Al-Laham, C. Y. Peng, A. Nanayakkara, M. Challacombe, P. M. W. Gill, B. Johnson, W. Chen, M. W. Wong, C. Gonzalez, J. A. Pople, Gaussian, Inc., Wallingford CT, **2004**.

[10] a) H.-J. Kim, S. Sakamoto, K. Yamaguchi, J.-I. Hong, *Org. Lett.* **2003**, *5*, 1051; b) H. Y. Lee, H.-J. Kim, K. J. Lee, M. S. Lah, J.-I. Hong, *CrystEngComm* **2007**, *9*, 78.

[11] a) P. Samorí, V. Francke, T. Mangel, K. Müllen, J. P. Rabe, *Opt. Mater.* **1998**, *9*, 390; b) A. Ajayaghosh, R. Varghese, S. Mahesh, V. K. Praveen, *Angew. Chem.* **2006**, *118*, 7893; *Angew. Chem. Int. Ed.* **2006**, *45*, 7729.

[12] a) I. O. Shklyarevskiy, P. Jonkheijm, P. C. M. Christianen, A. P. H. J. Schenning, E. W. Meijer, O. Henze, A. F. M. Kilbinger, W. J. Feast, A. D. Guerzo, J.-P. Desvergne, J. C. Maan, *J. Am. Chem. Soc.* **2005**, *127*, 1112; b) M. Yang, W. Wang, F. Yuan, X. Zhang, J. Li, F. Liang, B. He, B. Minch, G. Wegner, *J. Am. Chem. Soc.* **2005**, *127*, 15107.

[13] a) F. M. Menger, A. V. Peresypkin, *J. Am. Chem. Soc.* **2003**, *125*, 5340; b) N. S. S. Kumar, S. Varghese, G. Narayan, S. Das, *Angew. Chem.* **2006**, *118*, 6465; *Angew. Chem. Int. Ed.* **2006**, *45*, 6317.

[14] For selected examples of gels developed through spherical aggregates, see: a) A. Nagai, J. Miyake, K. Kokado, Y. Nagata, Y. Chujo, *J. Am. Chem. Soc.* **2008**, *130*, 15276; b) I. A. Coates, D. K. Smith, *Chem. Eur. J.* **2009**, *15*, 6340; c) J. Wu, T. Yi, T. Shu, M. Yu, Z. Zhou, M. Xu, Y. Zhou, H. Zhang, J. Han, F. Li, C. Huang, *Angew. Chem.* **2008**, *120*, 1079; *Angew. Chem. Int. Ed.* **2008**, *47*, 1063; d) J. Liu, P. He, J. Yan, X. Fang, J. Peng, K. Liu, Y. Fang, *Adv. Mater.* **2008**, *20*, 2508; e) Y. Jeong, M. K. Joo, Y. S. Sohn, B. Jeong, *Adv. Mater.* **2007**, *19*, 3947; f) W. Weng, J. B. Beck, A. M. Jamieson, S. J. Rowan, *J. Am. Chem. Soc.* **2006**, *128*, 11663. Also see references [6a] and [13].

[15] D. Bardelang, F. Camerel, J. C. Margeson, D. M. Leek, M. Schmutz, M. B. Zaman, K. Yu, D. V. Soldatov, R. Ziessel, C. I. Ratcliffe, J. A. Ripmeester, *J. Am. Chem. Soc.* **2008**, *130*, 3313.

[16] For selected examples of a morphological transformation between vesicular and tubular structures, see: a) X. Yan, Q. He, K. Wang, L. Duan, Y. Cui, J. Li, *Angew. Chem.* **2007**, *119*, 2483; *Angew. Chem. Int. Ed.* **2007**, *46*, 2431; b) C. Wang, S. Yin, S. Chen, H. Xu, Z. Wang, X. Zhang, *Angew. Chem.* **2008**, *120*, 9189; *Angew. Chem. Int. Ed.* **2008**, *47*, 9049; c) J.-H. Ryu, D.-J. Hong, M. Lee, *Chem. Commun.* **2008**, 1043; d) X. Yan, Y. Cui, Q. He, K. Wang, J. Li, W. Mu, B. Wang, Z.-C. Ou-yang, *Chem. Eur. J.* **2008**, *14*, 5974; e) P. Sunintaboon, K. M. Ho, P. Li, S. Z. D. Cheng, F. W. Harris, *J. Am. Chem. Soc.* **2006**, *128*, 2168.

[17] a) P. Terech, R. G. Weiss, *Chem. Rev.* **1997**, *97*, 3133; b) M. George, R. G. Weiss, *Acc. Chem. Res.* **2006**, *39*, 489; c) N. M. Sangeetha, U. Maitra, *Chem. Soc. Rev.* **2005**, *34*, 821; d) L. A. Estroff, A. D. Hamilton, *Chem. Rev.* **2004**, *104*, 1201; e) K. J. C. van Bommel, A. Friggeri, S. Shinkai, *Angew. Chem.* **2003**, *115*, 1010; *Angew. Chem. Int. Ed.* **2003**, *42*, 980.

[18] T. Naota, H. Koori, *J. Am. Chem. Soc.* **2005**, *127*, 9324.

[19] For selected examples of ultrasound-triggered gels, see: a) K. M. Anderson, G. M. Day, M. J. Paterson, P. Byrne, N. Clarke, J. W. Steed, *Angew. Chem.* **2008**, *120*, 1074; *Angew. Chem. Int. Ed.* **2008**, *47*, 1058; b) C. Baddeley, Z. Yan, G. King, P. M. Woodward, J. D. Badjić, *J. Org. Chem.* **2007**, *72*, 7270; c) K. Isozaki, H. Takaya, T. Naota, *Angew. Chem.* **2007**, *119*, 2913; *Angew. Chem. Int. Ed.* **2007**, *46*, 2855; d) J. M. J. Paulusse, R. P. Sijbesma, *Angew. Chem.* **2006**, *118*, 2392; *Angew. Chem. Int. Ed.* **2006**, *45*, 2334; e) C. Wang, D. Zhang, D. Zhu, *J. Am. Chem. Soc.* **2005**, *127*, 16372. Also see references [14c], [14d], and [15].

[20] S. Zhang, S. Yang, J. Lan, Y. Tang, Y. Xue, J. You, *J. Am. Chem. Soc.* **2009**, *131*, 1689.

[21] a) J. Seo, J. W. Chung, E.-H. Jo, S. Y. Park, *Chem. Commun.* **2008**, 2794; b) D. G. Velázquez, D. D. Díaz, A. G. Ravelo, J. M. Tellado, *J. Am. Chem. Soc.* **2008**, *130*, 7967; c) R. Oda, F. Artzner, M. Laguerre, I. Huc, *J. Am. Chem. Soc.* **2008**, *130*, 14705.

[22] A. Kraft, F. Osterod, *J. Chem. Soc. Perkin Trans. 1* **1998**, 1019.

[23] a) E. A. Mash, K. A. Nelson, S. van Deusen, S. B. Hemperly, *Org. Synth. Coll. Vol. 8* **1993**, 155; b) A. Salvini, P. Frediani, E. Rivalta, *Inorg. Chim. Acta* **2003**, *351*, 225; c) J. J. Bou, A. Rodriguez-Galán, S. Muñtoz-Guerra, *Macromolecules* **1993**, *26*, 5664.

Received: October 6, 2009
Published online: January 11, 2010

